Temperature-dependent diffusion coefficients from *ab initio* computations: Hydrogen, deuterium, and tritium in nickel

Erich Wimmer,* Walter Wolf, Jürgen Sticht,† and Paul Saxe
Materials Design, Inc., Angel Fire, New Mexico 87710, USA

Clint B. Geller
Bechtel Bettis, Inc., West Mifflin, Pennsylvania 15122, USA

Reza Najafabadi and George A. Young
Lockheed Martin Corporation, Schenectady, New York 12301-1072, USA

(Received 16 November 2007; revised manuscript received 29 February 2008; published 11 April 2008)

The temperature-dependent diffusion coefficients of interstitial hydrogen, deuterium, and tritium in nickel are computed using transition state theory. The coefficient of thermal expansion, the enthalpy and entropy of activation, and the pre-exponential factor of the diffusion coefficient are obtained from *ab initio* total energy and phonon calculations including the vibrations of all atoms. Numerical results reveal that diffusion between octahedral interstitial sites occurs along an indirect path via the metastable tetrahedral site and that both the migration enthalpy and entropy are strongly temperature dependent. However, the migration enthalpy and entropy are coupled so that the diffusion coefficient is well described by a constant activation energy, i.e., $D=D_0\exp[-Q/(RT)]$, with $Q=45.72$, 44.09, and 43.04 kJ/mol and $D_0=3.84\times10^{-6}$, 2.40×10^{-6}, 1.77×10^{-6} $m^2\,s^{-1}$ for H, D, and T, respectively. The diffusion of deuterium and tritium is computed to be slower than that of hydrogen only at temperatures above 400 K. At lower temperatures, the order is reversed in excellent agreement with experiment. The present approach is applicable to atoms of any mass as it includes the full coupling between the vibrational modes of the diffusing atom with the host lattice.

DOI: 10.1103/PhysRevB.77.134305 PACS number(s): 66.30.Dn, 63.20.D−, 65.40.G−

I. INTRODUCTION

Diffusion in solids is of broad interest and fundamental importance for understanding the properties of materials, including segregation, phase transformations, hydrogen embrittlement, and corrosion. Despite this importance, there is a serious lack of reliable experimental mass diffusion data. For example, experimental values for the diffusion coefficient of hydrogen in metals such as titanium[1] and aluminum[2] are scattered over many orders of magnitude and values for many important systems are not reported in the literature at all. Only in a few cases, such as hydrogen and its isotopes in nickel, experimental data from different groups are reasonably consistent to serve as reliable benchmark for computational approaches.[3–8]

As a result of progress in *ab initio* computational methods, it is now possible to calculate an increasing number of materials properties at a level of accuracy close to and sometimes better than available from experiment. The present work demonstrates that this can be achieved for the diffusion of hydrogen and its isotopes in nickel. The approach is based on *ab initio* theory and it is applicable to a range of diffusion mechanisms, including interstitial, vacancy assisted, ring, and interstitialcy diffusion. The computations provide insight into the thermodynamic aspects of the diffusion process including the change of the vibrational entropy of the entire system between the stable state and the transition state as a function of temperature.

Ab initio methods at various levels of approximation have been used in the study of solid-state diffusion[9–17] and found to be highly valuable. In this context, the diffusion of H in metals is of particular interest, as recently reviewed by Sholl.[17] However, no previously reported study has taken advantage of *ab initio* phonon calculations of the entire system to obtain enthalpies and entropies as a function of temperature, thus including the coupling of the phonons of the host lattice with the vibrations of the diffusing H atoms. While this coupling can be included by combining a thermodynamical integration method with *ab initio* molecular dynamics, as demonstrated by Milman *et al.*,[11] such an approach is computationally very demanding and simulations have to be explicitly performed for each temperature, while a quasiharmonic phonon approach provides information for a large temperature range in a single set of calculations. Furthermore, effects due to thermal expansion are often not taken into account but can be treated consistently within a quasiharmonic phonon approach. In fact, it is current practice in *ab initio* computations of hydrogen diffusion in solids to use the electronic energy of the relaxed structures of the ground state and transition state as reference and then to consider only the vibrations of the H atom in deriving the zero-point energy corrections and the vibrational partition functions, as done, for example, in Ref. 15. In such an approach, the full coupling with the host lattice and effects due to thermal expansion are neglected. It is the purpose of the present work to gain a deeper understanding of these effects on the accuracy of computed diffusion coefficients, thus providing also a firmer basis for assessing the accuracy of the electronic energy for transition states and reaction barriers, as obtained from density functional calculations.

The present work is based on Eyring's[18] concept of the activated complex, as applied by Wert and Zener[19] to impu-

rity diffusion in solids. Density functional theory combined with the direct approach for phonon dispersions is employed in the *ab initio* computation of the energy hypersurface, vibrational frequencies, activation enthalpy, and the activation entropy. All vibrational degrees of freedom of the entire supercell are taken into account. In addition, effects due to thermal expansion are included in a self-consistent manner. This establishes a framework for computing the temperature-dependent diffusion coefficients of general applicability, which is demonstrated in the present work for the case of interstitial diffusion of hydrogen, deuterium, and tritium atoms in crystalline nickel.

The value of a general and reliable computational approach for diffusion coefficients depends on a clear understanding and control of all possible sources of errors. At today's state of electronic structure theory, a serious concern is the accuracy of the present level of gradient-corrected density functionals in describing the height of diffusion barriers. This question cannot be properly answered unless all other sources of errors are investigated, which may cloud such an assessment. These include (i) the identification of the relevant diffusion mechanism, (ii) the accuracy in treating the temperature-dependent thermodynamic functions, (iii) the role of lattice expansion due to thermal expansion and impurity-induced strains, and (iv) other effects such as quantum mechanical tunneling. Furthermore, the application of Eyring's[18] concept of the activated transition state complex involves several subtle approximations.

It is the aim of the present work to establish a better understanding of the importance of each of these aspects by a detailed investigation of a particular case, namely, the interstitial diffusion of hydrogen isotopes in nickel. It turns out that the present approach gives very satisfactory results for a wide temperature range, which is of particular relevance for industrial materials such as nickel-based alloys. Unless there is a very fortuitous cancellation of errors, the present results indicate that current gradient-corrected density functionals together with *ab initio* calculations of the thermodynamic functions provide a useful basis for the prediction of diffusion coefficients of impurities in solids at a level of accuracy, which is comparable to that obtained from experiment.

The subsequent chapters are organized as follows. The theoretical and computational framework is discussed in Sec. II. Results are presented in Sec. III. A discussion of the approximations and an assessment of their influence on the accuracy of the computed diffusion coefficient are given in Sec. IV. Section V presents the conclusions together with perspectives for this approach.

II. THEORETICAL FRAMEWORK

It is common practice to express the diffusion coefficient in the form

$$D = D_0 e^{-Q/kT}, \tag{1}$$

where Q is the height of the activation barrier, D_0 is a prefactor, which is often assumed to be independent of the temperature T, and k is the Boltzmann constant. Equation (1) is usually represented as an Arrhenius plot in the form $\ln(D) = \ln(D_0) - (Q/k)(1/T)$.

Following Wert and Zener,[19] the diffusion coefficient can be written as

$$D = n\beta d^2 \Gamma, \tag{2}$$

where n is the number of nearest-neighbor stable sites for the diffusing interstitial atom, β is the probability that a jump to a nearest-neighbor site leads forward in the direction of diffusion, and d is the length of the jump projected onto the direction of diffusion. Γ denotes the jump rate between adjacent sites of the diffusing particle.

In the present work, the *ab initio* computation of the jump rate is based on Eyring's[18] theory of the activated complex. There are several subtleties in this theory, which are worthwhile recalling in the context of diffusion in solids. Eyring's theory assumes that a reaction, or in the present case a diffusive jump, proceeds over a transition state, which is in thermodynamic equilibrium with its surrounding. Based on this fundamental assumption, the reaction rate is determined by (i) the ratio between the partition functions of the system in the transition state and the initial state including the Boltzmann factor $\exp[-\Delta E/(kT)]$, involving the activation energy ΔE, and (ii) the mean velocity of the reactants crossing the transition state. Besides the activation energy, the vibrational degrees of freedom at the transition state and the stable state determine the partition function.

In the present case, the activation energy is obtained from electronic structure total energy calculations. *Ab initio* phonon calculations provide all vibrational terms, i.e., the zero-point energy, the temperature-dependent part of the internal energy, and the vibrational entropy. The phonon calculations include all atoms of the system and not just the diffusing atom. Hence, the present approach takes into account the full coupling of the vibrational modes between the diffusing atom and the host lattice. Following Eyring,[18] the mean velocity for crossing the transition state is taken from the temperature-dependent velocity distribution of classical particles at a temperature T. The reaction (or jump) rate is then given by

$$\Gamma = \frac{kT}{h}\frac{Z_{TS}}{Z_0} e^{-\Delta E_{el}/kT}, \tag{3}$$

where the Z_{TS} and Z_0 are partition functions for the transition state and the ground state, respectively, ΔE_{el} is the difference in the minimum (electronic) energy of the transition state (E_{TS}) and of the ground state (E_0), and h is Planck's constant. Note that the free translational degree of freedom in the transition state is moved to the kT/h term and the partition function Z_{TS} has one degree of freedom less than Z_0.

Within the framework of the harmonic approximation, the quantum mechanical partition functions in Eq. (3) can be written as

$$\Gamma = \frac{kT}{h}\frac{\prod_{i=1}^{3N-6}\left[2\sinh\left(\frac{h\nu_i^0}{2kT}\right)\right]}{\prod_{i=1}^{3N-7}\left[2\sinh\left(\frac{h\nu_i^{TS}}{2kT}\right)\right]} e^{-\Delta E_{el}/kT}, \tag{4}$$

where ν_i^{TS} and ν_i^0 are the vibrational frequencies at the transition state and the ground state, respectively. For the high

temperature range ($h\nu/2kT \ll 1$), the jump rate reduces to the results found by Vineyard[20]

$$\Gamma = \frac{\Pi_{i=1}^{3N-6} \nu_i^0}{\Pi_{i=1}^{3N-7} \nu_i^{TS}} e^{-\Delta E_{el}/kT} = \nu^* e^{-\Delta E_{el}/kT}. \quad (5)$$

For the low temperature range ($h\nu/2kT \gg 1$), the jump rate can be written as

$$\Gamma = \frac{kT}{h} \frac{\exp \Sigma_{i=1}^{3N-6} \frac{h\nu_i^0}{2kT}}{\exp \Sigma_{i=1}^{3N-7} \frac{h\nu_i^{TS}}{2kT}} e^{-\Delta E_{el}/kT} = \frac{kT}{h} e^{-(\Delta E_{el}+\Delta E_{zp})/kT}, \quad (6)$$

where ΔE_{zp} is the difference in zero-point energies between ground state and transition state. In a periodic structure, one needs to integrate all phonon branches over the Brillouin zone. To this end, it is convenient to use the relationships

$$G_{vib} = -kT \ln Z_{vib} = kT \int_0^\infty g(\nu) \ln \left[2 \sinh \left(\frac{h\nu}{2kT} \right) \right] d\nu, \quad (7)$$

where G_{vib} denotes the vibrational terms of the free energy (including the zero-point energy) and $g(\nu)$ is the phonon density of states of the periodic system. With this, the jump rate can be written as

$$\Gamma = \frac{kT}{h} e^{-\Delta G_{vib}/kT} e^{-\Delta E_{el}/kT}. \quad (8)$$

In the case of interstitial diffusion in a fcc lattice of lattice parameter a with the octahedral site as the ground state, the diffusion coefficient is given by

$$D = a^2 \Gamma = a^2 \frac{kT}{h} e^{-(\Delta E_{el}+\Delta G_{vib})/kT} = a^2 \frac{kT}{h} e^{-\Delta G_{TS-oct}/kT}. \quad (9)$$

If the tetrahedral interstitial site is sufficiently deep, as is the case for H in Ni, it is reasonable to assume that the diffusing atom temporarily equilibrates in the tetrahedral site before jumping forward or backward to a neighboring octahedral site. Inclusion of this equilibration leads to the following form of the diffusion coefficient:

$$D_1 = D \frac{1}{2} (1 + 2e^{-\Delta G_{tet\text{-}oct}/kT})^{-1}. \quad (10)$$

This expression is obtained from an analysis of the forward and backward steady-state fluxes across the energy divides, which separate octahedral and tetrahedral sites. It is assumed that the distribution of hydrogen atoms between adjacent octahedral and tetrahedral interstitial sites is governed by a local thermodynamic equilibrium, thus introducing the difference in the free energy between hydrogen in tetrahedral and octahedral sites, $\Delta G_{tet\text{-}oct}$. The factor 2 arises from the fact that in a fcc lattice, there are two tetrahedral interstitial sites for each octahedral site.

The electronic energies in the above expressions are computed with density functional theory[21] in its spin-polarized form[22] with the generalized gradient approximation[23] and all-electron frozen-core projector-augmented-wave potentials,[24] as implemented in the Vienna *ab initio* simulation package (VASP).[25] Thermodynamic functions are obtained from phonon dispersions, which are computed by the direct method[26] with *ab initio* forces from VASP as integrated in the MEDEA computational environment.[27]

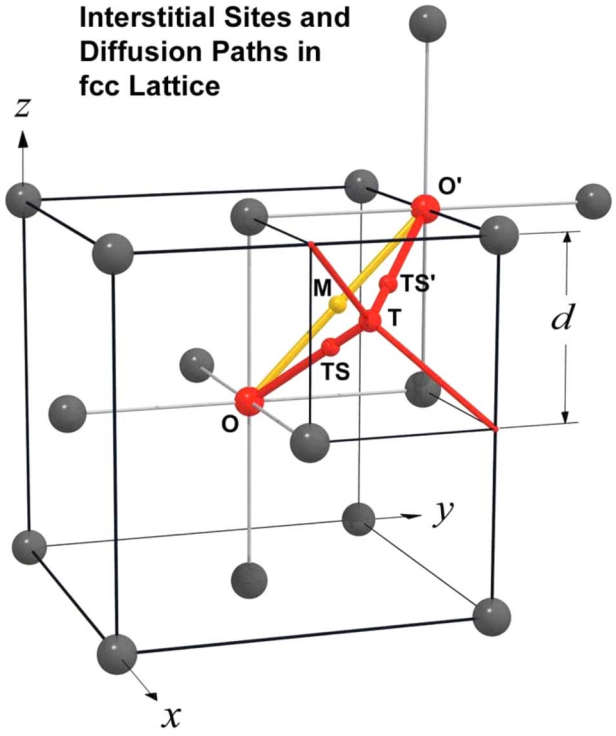

FIG. 1. (Color online) Conventional fcc unit cell with an interstitial impurity atom diffusing from an octahedral site O a distance d in the z direction to a nearest-neighbor octahedral site O′. M is the midpoint between O and O′; T denotes a tetrahedral interstitial site. The equivalent transition states are labeled TS and TS′.

The system is described by a $2\times2\times2$ Ni supercell containing 32 host atoms and one H impurity. In the geometry optimizations and the evaluation of the electronic energies, the one-particle wave functions are expanded in a plane wave basis with a cut off energy of 337 eV. Integrations over the Brillouin zone are performed by using a $5\times5\times5$ Monkhorst–Pack k mesh and a tetrahedron scheme with Blöchl corrections. In the phonon calculations, a non-spin-polarized Hamiltonian is used, the $5\times5\times5$ k mesh is maintained, and the plane wave cutoff is 270 eV.

The transition state is determined by first exploring the energy hypersurface in the form of constrained geometry optimizations, i.e., by placing the H atom at the potentially relevant interstitial sites and by relaxing the surrounding atoms. From this analysis, a position of the H atom near the (111) plane of Ni atoms between the octahedral and tetrahedral sites is identified as the likely transition state. Starting with the H atom in the (111) plane of Ni atoms between the octahedral and tetrahedral sites, all positions of all atoms of the supercell are relaxed such that all forces on all atoms are smaller than 0.01 eV/Å. This is accomplished using the residual minimization—direct inversion in the iterative subspace algorithm,[28] as implemented in VASP. In this algorithm, only forces and not the total energy are used so that the system can climb to a saddle point, which is a stationary

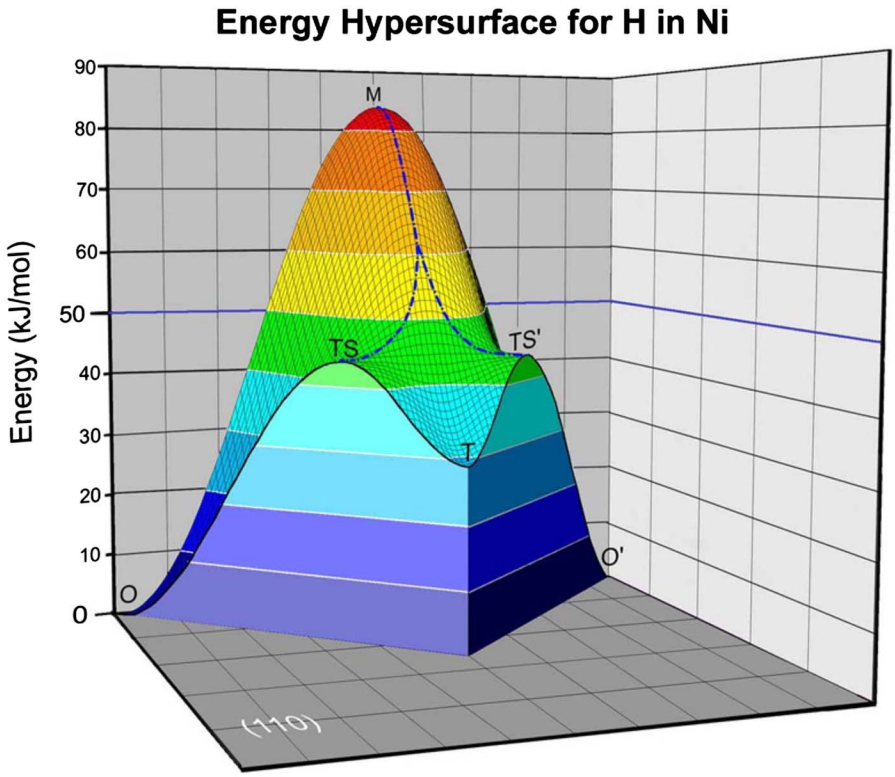

FIG. 2. (Color online) Energy hypersurface of H diffusing in nickel between octahedral interstitial sites. Note the pronounced local minimum at the tetrahedral site (T) and two transition states (TS and TS′) along the path from O to O′. The dashed-dotted line is the energy divide.

state with vanishing forces for all atoms. Due to the high symmetry and geometric simplicity of the present system, it is not necessary to use methods such as the nudged elastic band algorithm to find the transition state. However, for completeness, such a nudged elastic band calculation has been performed leading to exactly the same result as the procedure described above.

The coefficient of thermal expansion is determined from a minimization of the free energy as a function of temperature and lattice parameter.[29] To this end, 17 phonon calculations are performed for a Ni lattice with the lattice parameter $a = 3.50, 3.51, 3.52, \ldots, 3.66$ Å. For each of these values, the vibrational free energy is computed from the phonon density of states and combined with highly precise electronic energies (spin polarized, 500 eV plane wave cutoff, $21 \times 21 \times 21$ k mesh, and tetrahedron integration with Blöchl corrections). The phonon calculations for the thermal expansion are performed with the same computational parameters as those for the diffusion coefficients.

III. RESULTS

A. Structural and thermodynamic properties

For pure nickel, the present calculations give a lattice parameter of 3.5197 Å at $T=0$ K, which is 0.1% larger than the experimental value[30] when extrapolated from room temperature (3.5238 Å) to zero temperature (3.517 Å). The quasiharmonic approach that is described above provides a good prediction of the coefficient of thermal expansion (CTE) of bulk Ni. In particular, the computed CTE of Ni at room temperature is 11.9×10^{-6} K^{-1} compared to experimental values of 12.7×10^{-6} K^{-1} (Ref. 31) and 12.9×10^{-6} K^{-1}.[32] At 1200 K, the computed value increases to 16.5×10^{-6} K^{-1} compared to an experimental value of 20.1×10^{-6} K^{-1}.[32] For the present purpose, the computed values for the temperature-dependent lattice parameter are described by the following polynomial fit:

$$a(T) = 3.5197 + 2.77\,421 \times 10^{-5} T + 2.28\,245 \times 10^{-8} T^2 - 5.24\,331 \times 10^{-12} T^3 + 3.62\,986 \times 10^{-16} T^4 \ (\text{Å}). \quad (11)$$

This establishes a consistent reference for the structural parameters of bulk nickel as a function of temperature.

Using the structural parameter of pure nickel at $T=0$ K, a $2 \times 2 \times 2$ supercell is constructed and one hydrogen impurity is placed at the octahedral (O) and tetrahedral (T) interstitial sites, near the transition state (TS), and at the local maximum between two octahedral sites (M), as illustrated in Fig. 1. All atomic positions in each of the 33-atom supercells are relaxed until the largest force on any atom is smaller than 0.01 eV/Å. The lattice parameters of the supercells are kept at the computed value of a pure nickel crystal. The resulting energy hypersurface shows that the lowest-energy path from one octahedral site to an adjacent site leads over a transition state, which is located between the tetrahedral and the octahedral sites, as illustrated in Fig. 2. An important feature of the energy hypersurface of interstitial H in Ni is a pronounced local minimum at the tetrahedral site. The shortest path between two adjacent octahedral sites leads over the point M, where a diffusing atom would be exactly at the midpoint of a Ni-Ni bond. The electronic energy of this point is a maximum on the energy divide, as shown in Fig. 2. The critical points on the energy hypersurface are therefore the

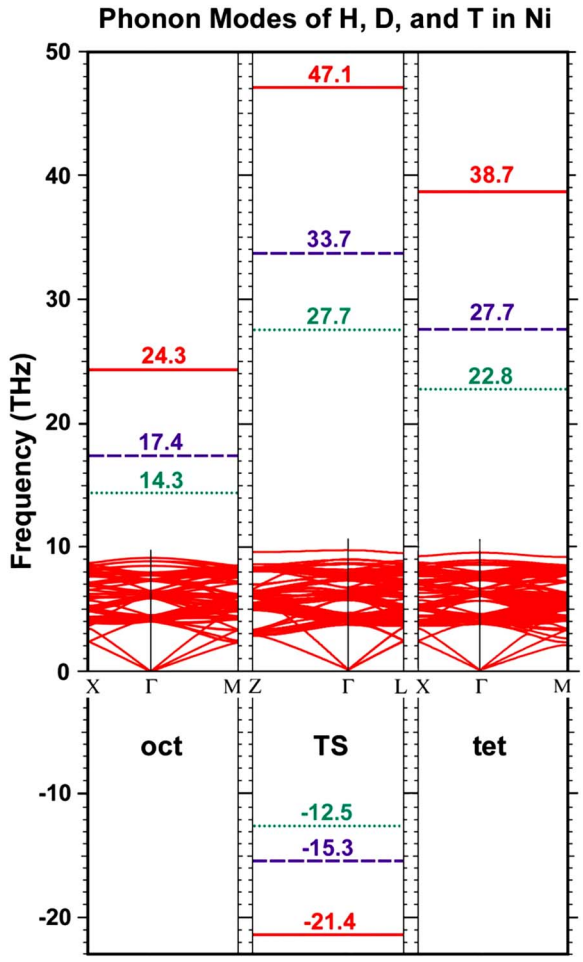

FIG. 3. (Color online) Computed phonon dispersions of a 32-atom Ni supercell with H, D, and T atoms in the stable octahedral site (oct), the transition state (TS), and the metastable tetrahedral site (tet), respectively. The computations were performed for a lattice constant of $a=3.5197$ Å. The isolated, dispersionless phonon branches are related to vibrations of the H, D, and T atoms (solid, broken, and dotted lines). The modes with imaginary frequencies at the transition state (plotted as negative frequency) correspond to the motion of the H, D, and T atoms across the barrier. The symmetry of the supercell describing the TS state is different from that of the octahedral and tetrahedral sites, which is reflected in the labeling of the special points in the Brillouin zone.

stable octahedral site, the transition state, and the metastable tetrahedral sites. The calculations reveal that the transition state is not located exactly in a (111) plane of Ni atoms, as one might expect from a pure geometric consideration, but it is 0.07 Å outside this plane on the side of the octahedral site. The reason is a slight attraction between the H atom and the Ni atom at position (a, a, a) (cf. Fig. 1), which is counterbalanced by a repulsive force from the three closest Ni atoms.

The phonon dispersions of 32-atom Ni supercells with a hydrogen atom at each of these three characteristic sites are shown in Fig. 3. When a hydrogen atom occupies an octahedral interstitial site, then the phonon dispersions show a threefold degenerate dispersionless branch at 24.3 THz, which corresponds to the very weakly coupled vibration of the interstitial hydrogen atom. All phonon frequencies are real, indicating a true minimum on the energy hypersurface. When the hydrogen atom moves to the transition state, the highest H-related frequency is shifted to 47.1 THz. This doubly degenerate mode corresponds to a vibration of the H atoms perpendicular to the diffusion path. By definition, a transition state is characterized by the occurrence of one negative eigenvalue in the dynamical matrix. This corresponds to a motion of the H atom along the diffusion path. This mode has an imaginary frequency, which is plotted as a "negative" frequency at −21.4 THz. The magnitude of the curvature of the energy hypersurface across the transition barrier is nearly the same as the curvature around the minimum at the octahedral site (compare 21.4 and 24.3 THz). Inspection of the hypersurface (Fig. 2) makes this plausible. The energy profile along the diffusion path from the stable site to the transition state is well described by a sinusoidal energy profile, as originally suggested by Wert and Zener.[19] When the tetrahedral site is occupied, all phonon branches are positive indicating a local minimum. Due to the confined interstitial space in a tetrahedral site, the corresponding vibrational mode of an H atom has a higher frequency, namely, 38.7 THz, compared to 24.3 THz in an octahedral site. At the transition state and, to a somewhat lesser extent at the tetrahedral site, there is a phonon branch between 9 and 10 THz, which is split off from the bulk of Ni-related phonon branches (cf. Fig. 3). This branch is related to motions of Ni atoms, which couple with motions of the H impurity. Integration of the phonon dispersion over the entire Brillouin zone leads to phonon densities of states, thus allowing the evaluation of the zero-point energy, the temperature-dependent enthalpy, entropy, and free energy.

The phonon calculations are repeated for a lattice expanded by 2.1% ($a=3.5936$ Å), which corresponds to a temperature of 1450 K. The total energies and thermodynamic functions are then interpolated between the results from the two reference lattice parameters, thus taking into account thermal expansion. Upon expansion of the Ni lattice the energy barrier decreases, as does the energy difference between the tetrahedral and the octahedral sites (cf. Table I). As expected, an expansion of the lattice leads to a softening of vibrational modes. For example, the frequency of the H atom in the stable octahedral site is shifted from 24.3 to 20.6 THz if the lattice is expanded by 2.1%.

The dependence of the enthalpy and entropy on the temperature and the effect of lattice expansion are investigated next. To this end, we take differences between the thermodynamic functions at the transition state and the octahedral ground state. The results are shown in Fig. 4. The enthalpy difference remains nearly constant at low temperatures and then steadily decreases for temperatures above room temperature. At low temperatures, the vibrational entropy is larger when the H impurity occupies the transition state compared with the octahedral site. At temperatures above 500 K, the reverse is the case as the entropy in the octahedral geometry increases faster than that of the transition state.

In their original work, Wert and Zener[19] assumed the term ΔS to be positive, arguing that an impurity at the transition state might lower the shear modulus of the host lattice, which would lead to an increase in the entropy. The present calcu-

TABLE I. Computed electronic energy E_{el} and zero-point energy E_{zp} for interstitial hydrogen, deuterium, and tritium impurities in bulk nickel. All energies are in kJ/(mol of $Ni_{32}X$). The electronic energy of the elements in their standard state is taken as reference. The vibrational frequency of the impurity at the transition state is given as an imaginary value corresponding to the mode along the diffusion path. The values in the octahedral and tetrahedral sites are threefold degenerate and there are two degenerate modes with positive frequencies at the transition state.

	Ni_{32}	$Ni_{32}X$(oct)	$Ni_{32}X$(TS)	TS-oct	$Ni_{32}X$(tet)	tet-oct
			a=3.5197 Å			
Hydrogen						
E_{el}	0	7.32	46.49	39.17	31.96	24.64
E_{ZP}	112.64	128.23	131.93	3.70	136.37	8.14
ν_H (THz)		24.3	21.4*i*, 47.1		38.7	
Deuterium						
E_{ZP}		124.02	126.75	2.73	129.95	5.93
ν_H (THz)		17.4	15.3*i*, 33.7		27.7	
Tritium						
E_{ZP}		122.08	124.26	2.18	126.99	4.91
ν_H (THz)		14.3	12.5*i*, 27.7		22.8	
			a=3.5936 Å			
Hydrogen						
E_{el}	74.01	66.19	95.95	29.76	82.84	16.65
E_{ZP}	103.04	113.20	117.20	4.00	121.47	8.27
ν_H (THz)		20.6	19.6*i*, 43.2		35.8	
Deuterium						
E_{ZP}		109.71	112.08	2.37	115.30	5.59
ν_H (THz)		14.7	14.0*i*, 30.9		25.6	
Tritium						
E_{ZP}		108.12	109.92	1.80	112.52	4.40
ν_H (THz)		12.1	11.5*i*, 25.3		21.1	

lations show that the situation is more complicated due to the strong temperature dependence of the migration entropy. In the free energy, the decrease in ΔH is offset by the entropy term $-T\Delta S$ so that the free energy difference between the transition state and the stable state steadily decreases over the entire temperature range with a smaller slope than the enthalpy. Figure 4 also illustrates the fact that the zero-point energy of the system at the transition state is higher than at the stable octahedral site (cf. Table I).

The difference in the electronic energy (enthalpy) of the transition state and the octahedral site computed for the lattice at T=0 K is close to the difference in the free energy $\Delta G(T)$ around 500 K, which corresponds to the temperature where the difference in the entropy changes from positive values at low temperature to negative values at high temperature. A thermal expansion of the lattice lowers the diffusion barrier and increases the entropy of the transition state, as shown in Fig. 4. The differences shown in Fig. 4 are taken between two systems, where the reference state has one more vibrational degree of freedom than the transition state. This is consistent with Eq. (4).

The temperature-dependent difference of the free energy between the tetrahedral and the octahedral sites $\Delta G_{tet\text{-}oct}$ decreases almost linearly with temperature. Hence, a noticeable fraction of interstitial hydrogen atoms occupy tetrahedral sites at elevated temperature. For example, at 1000 K about 9% of all interstitial H atoms occupy tetrahedral sites.

B. Diffusion coefficient

In the present work, the temperature-dependent diffusion coefficient of H in Ni including equilibration in the metastable tetrahedral site is given by

$$D_1 = a^2 \frac{kT}{h} e^{-(\Delta E_{el}+\Delta G_{vib})/kT} \frac{1}{2}(1+2e^{-\Delta G_{tet\text{-}oct}/kT})^{-1}, \quad (12)$$

as explained in Sec. II. Effects due to thermal expansion are included in the lattice parameter and the free energy terms.

The computed diffusion coefficient D_1 is in remarkable agreement with the available experimental data, as can be seen from Fig. 5. At low temperatures, the computed diffusion coefficient falls well in the middle of the scattered experimental data. At elevated temperatures, D_1, is higher than the experimental data.

The Arrhenius plot of the computed diffusion coefficient (Fig. 5) shows a remarkably linear behavior and thus we can compute an effective activation barrier and a prefactor. From Eq. (1), we obtain

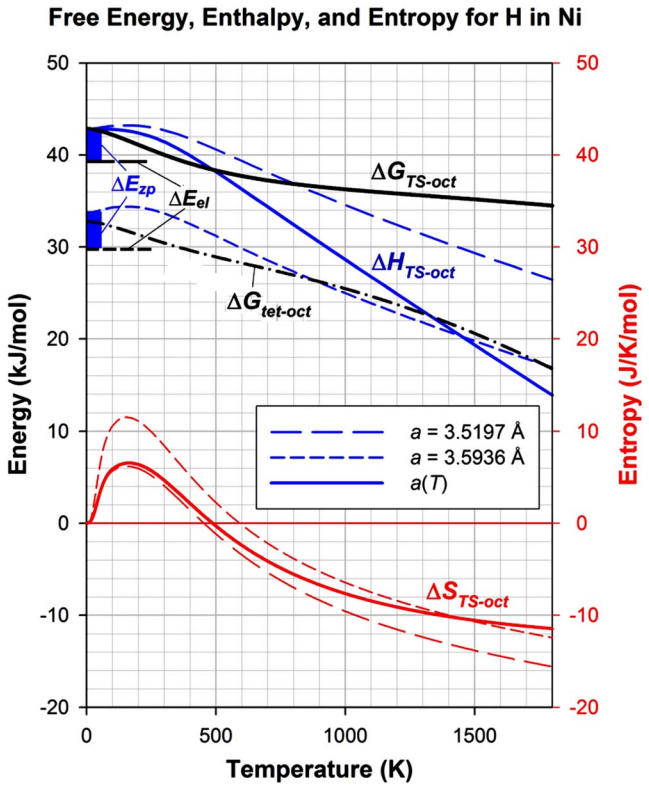

FIG. 4. (Color online) Differences of the free energy (ΔG), enthalpy (ΔH), and entropy (ΔS) between the transition state and the stable octahedral site as a function of temperature and lattice parameter. The changes in the electronic energy (ΔE_{el}) and the zero-point energy (ΔE_{zp}) are shown in connection with the enthalpy in the upper left of the graph. The values corresponding to a lattice parameter of $a=3.5197$ and 3.5936 Å are shown in long- and short-dashed lines, respectively. The thermodynamic functions corresponding to a temperature-dependent lattice parameter are drawn as solid lines. The free energy difference between the tetrahedral and octahedral sites ($\Delta G_{tet\text{-}oct}$) is plotted as dashed-dotted line. This term includes effects due to thermal lattice expansion.

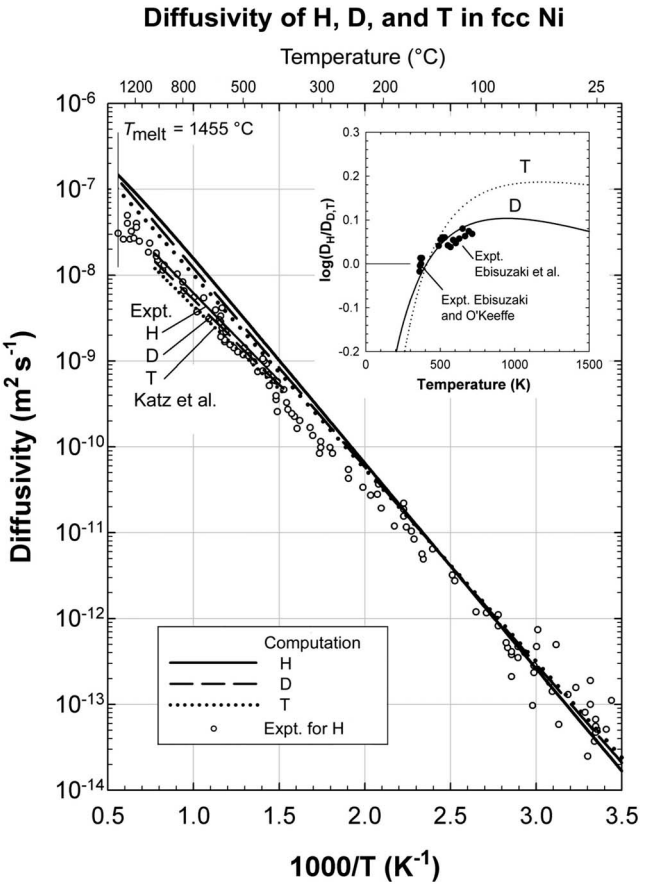

FIG. 5. Computed and experimental diffusion coefficient of H, D, and T in Ni. The computations are based on Eq. (12) including thermal expansion and equilibration in the tetrahedral sites. The experimental data for H (marked by open circles) are taken from Völkl and Alefeld (Ref. 7); the high-temperature values for all three isotopes are from measurements by Katz *et al.* (Ref. 6). The ratio of the diffusivity of H and D (shown in the inset) includes a comparison to data reported by Ebisuzaki *et al.* (Ref. 3) and Ebisuzaki and O'Keeffe (Ref. 4).

$$\ln(D) = \ln(D_0) - \frac{Q}{RT}. \tag{13}$$

A linear fit between 273 and 1000 K of the computed data for D_1 for H, D, and T gives

$$Q = 45.72, 44.09, \text{ and } 43.04 \text{ kJ/mol},$$
$$D_0 = 3.84 \times 10^{-6}, 2.40 \times 10^{-6}, 1.77 \times 10^{-6} \text{ m}^2 \text{ s}^{-1}. \tag{14}$$

This is the result from a full *ab initio* calculation of the temperature-dependent diffusion coefficient for interstitial hydrogen, deuterium, and tritium in bulk nickel. The approach is based on gradient corrected density functional theory, includes the full dynamical response of the host lattice to the presence of a diffusing impurity in the form of a quasiharmonic phonon approach, and takes into account equilibration in a metastable tetrahedral site.

The computed slope, ln (D_1) vs $(1/T)$, i.e., the effective activation barrier for H is slightly larger than the experimental data given by Völkl and Alefeld.[7] Fukai[8] reported experimental activation energies ranging from 38.6 kJ/mol at low temperature to 40.5 kJ/mol at high temperature with prefactors between 1.8×10^{-7} and 6.9×10^{-7} m^2 s^{-1}.

C. Isotope effects

Using the electronic structure results of hydrogen in nickel, it is straightforward to compute the phonon dispersions, thermodynamic functions, and hence the temperature-dependent diffusion coefficient for the isotopes deuterium and tritium in nickel. As expected, the frequencies decrease with increasing mass (cf. Table I). One would thus expect a lower diffusivity for the heavier isotopes. The computed results show that this is only the case at temperatures above 400 K (cf. Fig. 5). At lower temperatures, the ordering is reversed, as clearly displayed in the inset in Fig. 5. This *ab initio* result is in excellent agreement with the experimental data by Katz *et al.*,[6] Ebisuzaki *et al.*,[3] and Ebisuzaki and O'Keeffe.[4]

The explanation of this behavior is due to a balance between two effects, namely, the lower vibrational frequency and the lower zero-point energy for heavier isotopes. The lower frequency reduces the diffusion rate of the heavier isotopes linearly with temperature whereas the second effect increases the rate through an exponential dependence. From the present phonon calculations, we obtain a reduction of the zero-point energy difference $E_{zp}(\mathrm{TS})-E_{zp}(\mathrm{oct})$ from 3.70 kJ/mol for H to 2.73 kJ/mol for D and 2.18 kJ/mol for T, as listed in Table I. Due to the term $\exp[-\Delta E_{zp}/(RT)]$ in the jump rate, this zero-point energy effect is more pronounced at lower temperatures. In the present case, the balance is such that a crossover for deuterium vs hydrogen occurs around 400 K. The present calculations predict a very similar crossover temperature also for tritium, as illustrated in Fig. 5.

D. Assessment of approximations

In the following, we present the results of an analysis of the sensitivity of the computed diffusion coefficient on the theoretical assumptions and approximations. The first sensitivity test is related to the diffusion mechanism. It probes the effect of the equilibration in the metastable tetrahedral site. A neglect of the tetrahedral site amounts to the use of Eq. (9) for the diffusion coefficient. The result is a diffusion coefficient denoted as D_2 in Fig. 6. Except for the neglect of an equilibration in the tetrahedral site, all other assumptions and parameters are the same as in the computation of D_1. In particular, effects due to thermal lattice expansion are included. As expected, the diffusion coefficient D_2 is larger than D_1 since no retardation of the diffusing hydrogen atom in tetrahedral sites is considered. Neglect of the tetrahedral sites overestimates the diffusion coefficient by a factor between 2 and 3 over the entire temperature range. The slope, i.e., the effective activation barrier, essentially remains unchanged. Hence, only the pre-exponential factor in Eq. (1) is affected.

The effect of thermal expansion is probed by evaluating the diffusion coefficient according to Eq. (10) using electronic energies, frequencies, and thermodynamic functions only for the lattice parameter at $T=0$ K. Otherwise, all other assumptions and parameters are the same as for D_2. i.e., the equilibration in the tetrahedral site is not included. The resulting diffusion coefficient is denoted as D_3 in Fig. 6. The neglect of thermal expansion results in a smaller diffusion coefficient. As expected, the effect is most pronounced at elevated temperatures, where the computed diffusion coefficients without thermal expansion are almost three times smaller than with thermal expansion (compare D_2 and D_3 in Fig. 6). Even at room temperature, the effect is noticeable. In fact, at 300 K, inclusion of thermal expansion increases the computed diffusion coefficient by a factor of 1.7. By coincidence, the effect due to equilibration in the metastable tetrahedral site (D_2 vs D_1) and that due to thermal expansion (D_3 vs D_2) are of equal magnitude and of opposite sign so that D_1 and D_3 are superposed (cf. Fig. 6).

The next test probes the coupling of the phonon modes of the Ni lattice with the vibrations of the H atom. To this end,

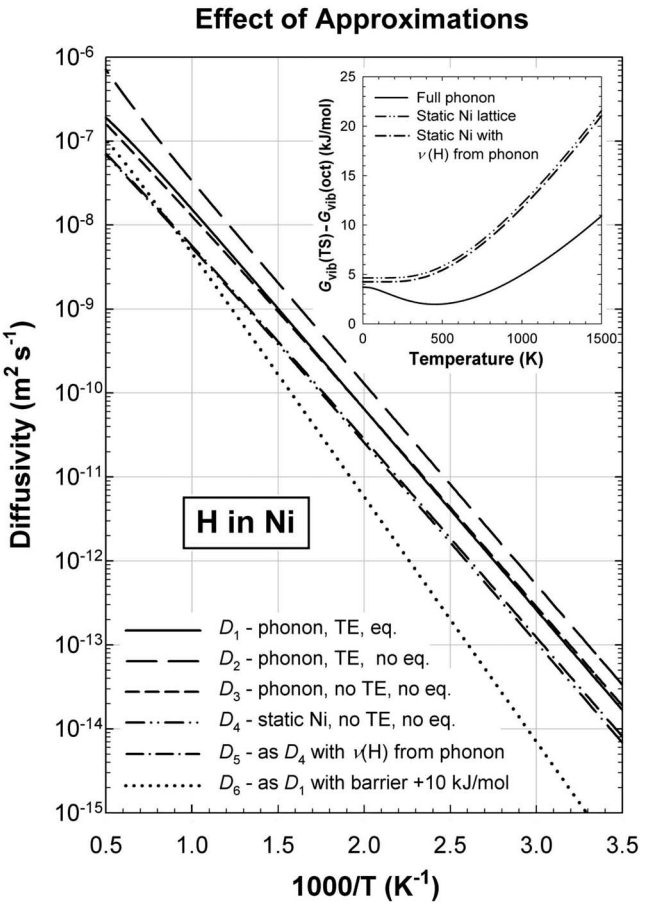

FIG. 6. Sensitivity of computed diffusion coefficient of H in Ni on the equilibration (eq.) in the metastable tetrahedral sites in the diffusion path, the effect of thermal expansion, the role of the vibrations of the Ni lattice, and the accuracy of the electronic energy in the computation of barrier heights.

the fully relaxed geometries for H in the octahedral sites and at the transition states are used to compute H frequencies while keeping the Ni lattice static. As expected, the frequencies obtained in this way deviate very little from the results of the full phonon calculations, as shown in Table II.

If one applies these vibrational frequencies of the H atom in computing the vibrational terms of the free energy of activation, i.e., the difference in the vibrational free energy of

TABLE II. Computed frequencies (in terahertz) of hydrogen, deuterium, and tritium in nickel using a full phonon approach and a static Ni lattice. The values in the octahedral sites are threefold degenerate and the second values at the transition state are twofold degenerate.

	H	D	T
	Full phonon		
ν_{oct}	24.3	17.4	14.3
ν_{TS}	21.4*i*, 47.1	15.3*i*, 33.7	12.5*i*, 27.7
	Static Ni lattice		
ν_{oct}	24.5	17.4	14.1
ν_{TS}	21.7*i*, 48.4	15.6*i*, 34.5	12.8*i*, 28.3

the transition state and the ground state using Eq. (4), then this energy difference is significantly larger than that obtained from a full phonon calculations, as illustrated in the insert in Fig. 6. As a consequence, the resulting diffusion coefficient computed within this approximation is smaller by a factor of 2.8 at room temperature and a factor of 2.4 at 1000 K compared to the results obtained from full phonon calculations (D_4 vs D_3). Inserting the vibrational frequencies of the H atom obtained from the full phonon calculations changes the picture only slightly (cf. D_4 and D_5 and the inset in Fig. 6). Hence, the difference must be attributed to the influence of the H atom on the phonons of the Ni lattice. The present results indicate a H-induced lowering of the contributions by the Ni lattice to the vibrational free energy of the transition state relative to the ground state. In other words, the H atom at the transition state decreases the vibrational free energy of the Ni atoms relative to the ground state, thus effectively lowering the pre-exponential term D_0.

The final sensitivity test probes the influence of the barrier height, i.e., the accuracy in the electronic structure calculations. To this end, the barrier height is artificially increased by 10 kJ/mol. Otherwise, all other assumptions and computational parameters are the same as in the case of D_1. The resulting diffusion coefficient, which is denoted as D_6 in Fig. 6 is substantially reduced, especially near room temperature. In fact, at 300 K, D_6 is 50 times smaller than D_1. The slope in the Arrhenius plot is very different from the experimental data and the previous cases (cf. Fig. 6). In other words, an artificial modification of the barrier height, i.e., a manipulation of the computed electronic energy destroys the agreement with experiment.

It is interesting that the slopes of diffusion coefficient curves (effective activation energies) for the temperature range shown in Fig. 6 are almost identical (~46 kJ/mol). To understand this observation and to identify the main contributions to the effective activation energy, we can simply separate (see Fig. 3) the effect of host atom vibrations and hydrogen atom vibrations on the jump rate in Eq. (4) as

$$\Gamma = \frac{kT}{h}\frac{\prod_{i=1}^{3N-9}\left[2\sinh\left(\frac{h\nu_i^0}{2kT}\right)\right]}{\prod_{i=1}^{3N-9}\left[2\sinh\left(\frac{h\nu_i^{TS}}{2kT}\right)\right]}\cdot\frac{\left[2\sinh\left(\frac{h\nu_i^0}{2kT}\right)\right]^3}{\left[2\sinh\left(\frac{h\nu_i^{TS}}{2kT}\right)\right]^2}e^{-\Delta E_{el}/kT}. \quad (15)$$

For the temperature range considered here, the $h\nu/2kT$ terms associated with Ni host atoms at both equilibrium and transition configuration are less than 1, while those corresponding to H diffusing atom fall in the 0.34–4.2 range. Equating the $\sinh(x)$ with x for those associated with host atoms in the jump rate equation results in the following diffusion coefficient:

$$D = a^2\frac{kT}{h}\frac{\Pi_{i=1}^{3N-9}\nu_i^0}{\Pi_{i=1}^{3N-9}\nu_i^{TS}}e^{-\Delta E_{el}/kT}\cdot\frac{\left[2\sinh\left(\frac{h\nu_H^0}{2kT}\right)\right]^3}{\left[2\sinh\left(\frac{h\nu_H^{TS}}{2kT}\right)\right]^2}. \quad (16)$$

From the above equation, it is clear that the temperature dependence of the hydrogen diffusion coefficient (effective activation energy) is essentially defined by terms involving the electronic energy, hydrogen vibrations, and kT, whereas the weakly temperature dependent lattice constant (a) and the vibrational terms of the host atoms determine the pre-exponential factor in the Arrhenius equation of hydrogen diffusion. Thus, hydrogen diffusion coefficients calculated including both thermal expansion and full phonon contribution (D_2), full phonon but no thermal expansion contribution (D_3), and only hydrogen vibrations contribution (D_4 and D_5) should lead to similar effective activation energy but different pre-exponential factors when fitted to an Arrhenius form. For the temperature range considered here, this behavior is clearly demonstrated in Fig. 6. To further assess the accuracy of the above approximation, we calculate various contributions to the effective activation energy.

The effective activation energy determined by fitting the above equation to an Arrhenius form can be separated into the contributions corresponding to the three temperature-dependent terms. These contributions can be calculated by fitting the individual terms to an exponential form. For the temperature range considered here, the contribution corresponding to the electronic term is obviously 39.2 kJ/mol (ΔE_{el}), the kT term leads to 3.9 kJ/mol, and the hydrogen vibrations term is 1.8 kJ/mol. The effective activation energy, i.e., the sum of these contributions is 44.9 kJ/mol, which is in very good agreement with the 45.7 kJ/mol value calculated using Eq. (4) which includes full phonon and thermal expansion contributions.

The good agreement between the effective activation energy determined using the above equation based on hydrogen vibrations only and that based on full phonon vibrations calculation using Eq. (4) suggests that the above approximation provides a simple and quite accurate method to calculate the activation energy.

It should be pointed out that the contribution of the hydrogen vibrations to the activation energy as noted above is 1.8 kJ/mol which is significantly different from the calculated zero-point energy, 4.25 kJ/mol. For the temperature range considered here, this shows that it is not correct to simply add the zero-point energy to the electronic energy to determine the effective activation energy. In fact, for temperatures where $h\nu/2kT \gg 1$ for hydrogen vibrations, as shown in Eq. (5), the activation energy is equal to the electronic energy and the zero-point energy has no contribution. For low temperatures where $h\nu/2kT \ll 1$ (corresponding to room temperature and lower in this study), as seen from Eq. (6), in addition to adding the zero-point energy to the electronic energy one needs to include the effect of the kT term to determine the effective activation energy.

IV. DISCUSSION

The results presented in the previous section demonstrate that the combination of transition state theory with accurate *ab initio* total energy and phonon calculations leads to a remarkable agreement between the computed and experimental temperature-dependent diffusion coefficient of hydrogen im-

purities in nickel. This result is based on the following assumptions and approximations: (i) the concentration of the impurity atoms is low, i.e., there are no interactions between the impurity atoms; (ii) the diffusion process is described by Eyring's transition state theory without dynamical corrections, i.e., each diffusing particle reaching a transition state also crosses it; (iii) no correlated multiple jumps (dynamical correlations) are considered; (iv) no quantum-mechanical tunneling effects are included, (v) the diffusing hydrogen atoms equilibrate in the metastable tetrahedral interstitial sites; (vi) electronic energies for both the ground state and the transition state are obtained from gradient-corrected density functional theory; and (vii) all vibrational terms to the partition function are obtained from a quasiharmonic phonon approach.

Within this framework, the sensitivity of the computed results have been analyzed for several key effects, namely, (i) the presence of metastable tetrahedral sites, (ii) thermal lattice expansion, (iii) the influence of the H impurity on the phonons of the Ni lattice, and (iv) the uncertainty in the computed barrier height due to possible errors in the electronic structure calculations. The analysis shows that in the case of H diffusion in Ni, the inclusion of equilibration in the metastable interstitial sites reduces the computed diffusion coefficient by about a factor of 2–3, while thermal expansion increases the diffusion coefficient by approximately the same factors.

The neglect of the vibrations of the Ni lattice by using only the H frequencies in the computation of the zero-point energy and vibrational partition functions leads to an error of a factor between 2 and 3 for the present case of H diffusion in Ni. This error is of the same magnitude as the effect of equilibration in the tetrahedral interstitial site and the effect of thermal expansion. In other words, the error from the assumption of a static host lattice is significant even though the ratio of the masses of H and Ni is 1:59. In the present system, the effect of the Ni lattice is mainly reducing the preexponential factor in the temperature range considered here (273–1000 K). Because of the complex nature of phonon dispersions in a solid, it is difficult to anticipate this effect, especially if the mass of the diffusing particle is similar to that of the host atoms.

The solubility of H in Ni at ambient pressure is below 0.01%.[33] Therefore, the assumption of a dilute limit is justified. Now, let us analyze the question of the appropriate diffusion mechanism. In his original paper, Eyring[18] introduced a factor c, which accounts for processes, when the activated complex crosses the transition barrier and then returns to the initial state. This dynamical-correction factor reduces the diffusion rate. Wert and Zener[18] implicitly set $c=1$. Later, this phenomenon was investigated by researchers including Bennett[34] and Voter,[35] revealing the complexity of this aspect.

The correlation of several diffusive jumps (dynamical correlations) represents another mechanism, which is not considered in the present approach. In fact, the results of Blöchl *et al.*[10] for the case of hydrogen diffusion in silicon seem to indicate that such dynamical correlations do not substantially affect the value for the diffusion coefficient. If such effects occur, they would tend to increase the effective diffusion coefficient and thus be opposite to the effect of dynamical-corrections mentioned above. For the temperature range of interest in the present work, namely, between room temperature up to high temperatures, it seems reasonable to keep the dynamical-correction factor $c=1$ and to neglect dynamical correlations.

A remaining concern is the quantum-mechanical tunneling. Building on the pioneering work by Flynn and Stoneham[36] and subsequent work on hydrogen diffusion in metals, a recent study by Sundell and Wahnström[14] on the diffusion of hydrogen in Nb and Ta demonstrates that for temperatures above 200 K the diffusion process can be described in terms of classical "overbarrier" motion. It is reasonable to assume that this conclusion also applies to the diffusion of hydrogen in Ni above room temperature.

The tetrahedral interstitial sites represent fairly deep local minima. With a vibrational frequency of 38.7 THz, we find the lowest vibrational level at 7.7 kJ/mol above the minimum with the first excited vibrational level being still inside the potential well of the tetrahedral site. Furthermore, a hydrogen atom diffusing from an octahedral site into a neighboring tetrahedral site has to change direction at the tetrahedral site before it can continue its path into the next octahedral site (cf. Fig. 1). These arguments make it plausible that H atoms equilibrate in the tetrahedral site at least at low and moderate homologous temperatures.

A critical term in the diffusivity is the effective height of the diffusion barrier. There is some evidence and also a widespread lore to the effect that the density functional theory–generalized gradient approximation (DFT-GGA) level of theory may underestimate barrier heights in reactions and that this may also apply to diffusion processes. The present results do not support this view. In fact, if one takes the full calculation including equilibration in tetrahedral sites and thermal expansion as reference (i.e., the case of D_1) and artificially increases the barrier height by 10 kJ/mol, the resulting diffusion coefficient significantly deviates from the experimental data both in terms of slope and, especially at lower temperatures, in absolute value, as illustrated in Fig. 6.

At high temperatures, nonharmonic vibrational effects may start to play a role. A comparison of the present computed results to experimental data indicates that the actual diffusion coefficient at high temperatures is lower than that predicted with the quasiharmonic approximation. This may indicate that the increasing vibrational disorder impedes the diffusion of hydrogen atoms compared to a quasiharmonic picture. In the regime of very high temperatures, the jump rate becomes sufficiently fast that *ab initio* molecular dynamics simulations may become more appropriate than a quasiharmonic approach based on transition state theory. Additionally, the effect of defects in real materials must be considered, e.g., vacancy and divacancy trapping states will act to lower the effective diffusivity of hydrogen at high homologous temperatures.

V. SUMMARY AND CONCLUSION

Transition state theory combined with an *ab initio* phonon approach has been applied to the diffusion of interstitial hy-

drogen, deuterium, and tritium in nickel. The key features of this approach are (i) vibrational coupling of the diffusing atoms with all surrounding host atoms are taken into account, (ii) the vibrational enthalpy and entropy terms are obtained over the entire temperature range of the solid phase with the diffusing atoms in the stable, metastable, and transition states, (iii) effects due to thermal expansion of the host lattice are included. The key conclusions are as follows.

(1) The computed energy profile for hydrogen and its isotopes in nickel reveals the octahedral interstitial position as the most stable site and diffusion between octahedral sites occurs indirectly via two transition states and the metastable tetrahedral site.

(2) The enthalpy and the entropy of migration, i.e., the difference between the values at the transition state and the stable state exhibit strong temperature dependence. Below 500 K, the entropy at the transition state is larger than in the ground state; at higher temperatures, the ordering is reversed.

(3) The effective activation energies as derived from an Arrhenius analysis of experimental data is in very good agreement with the computed effective activation energy that includes the effect of the full phonon vibrations, metastable tetrahedral sites, and thermal expansion. The computed diffusivity of hydrogen and its isotopes in nickel is well described by the form $D=D_0\exp[-Q/(RT)]$ with $Q=45.72$, 44.09, and 43.04 kJ/mol and $D_0=3.84\times10^{-6}$, 2.40×10^{-6}, 1.77×10^{-6} m^2 s^{-1} for H, D, and T respectively.

(4) The computed diffusivity of H relative to that of D and T is in excellent agreement with available experimental data. The present calculations give a quantitative explanation of the fact that D and T diffuse slower than H above 400 K but faster at lower temperature. The effect is due to a balance between a mass effect, which lowers the vibrational frequencies and thus diminishes the diffusivity and a zero-point energy effect, which lowers the effective barrier for the heavier isotopes thereby increasing the diffusion rate. The present calculations predict that the crossover in the diffusivity for tritium occurs at nearly the same temperature as that for D, namely, around 400 K.

(5) In the present case of H diffusion in Ni the neglect of the vibrations of the host lattice does not affect the activation energy in any substantial way, but it leads to an error of a factor of 2–3 in the pre-exponential coefficient. Therefore, the assumption of a static host lattice is a reasonable approximation for the diffusion of very light atoms in relatively rigid lattices of heavier atoms. However, even in this special case the effect of the host lattice can be quite noticeable. Hence, a static lattice approximation may lead to severe errors if applied to the diffusion of heavier atoms or the diffusion of hydrogen in a lattice of light atoms. The present approach overcomes this limitation, it is more general, but requires a higher computational effort.

(6) Provided that there is no fortuitous cancellation of errors or shortcomings in the present model, the results for the diffusion of H, D, and T in Ni suggest that the electronic energy difference of the diffusion barriers computed on the DFT-GGA level of theory are probably accurate to within 5 kJ/mol of experimental values. This estimate is based on a sensitivity analysis of the computed vs experimental diffusion coefficient.

In summary, a computational procedure for the *ab initio* calculation of diffusion coefficients in crystalline solids has been presented and demonstrated for the case of interstitial diffusion of hydrogen and its isotopes in nickel. At ambient and moderate temperatures, the agreement between computed and available experimental data is of the same magnitude as the scatter within the experimental results. Thus, the present *ab initio* approach for computing temperature-dependent diffusion coefficients provides a valuable tool for determining this important physical property at a level of accuracy, which is comparable to that obtained by experiment. This capability will be particularly useful in cases of large experimental uncertainties or for systems, where experiments are difficult to perform. The current computational technology and the automation of *ab initio* calculations of phonon spectra for large systems open exciting perspectives for this approach to compute this important physical property for a wide range of systems, thus contributing to a better understanding of a range of important processes including segregation, phase transformation, hydrogen embrittlement, and corrosion.

ACKNOWLEDGMENTS

The authors thank K. Parlinski for the collaboration on the phonon program and for valuable discussions with Bruce Eichinger (University of Washington) and Alexander Mavromaras (Materials Design).

*Corresponding author; ewimmer@materialsdesign.com
†Deceased.

[1] T. P. Papazoglou and M. T. Heppworth, Trans. Metall. Soc. AIME **242**, 682 (1968); E. Brauer *et al.*, Corros. Sci. **21**, 449 (1981).
[2] G. A. Young and J. R. Scully, Acta Mater. **46**, 6337 (1998), and references therein; C. Wolverton, V. Ozoliņš, and M. Asta, Phys. Rev. B **69**, 144109 (2004).
[3] Y. Ebisuzaki, W. J. Kass, and M. O'Keeffe, J. Chem. Phys. **46**, 1373 (1967).
[4] Y. Ebisuzaki and M. O'Keeffe, J. Chem. Phys. **48**, 1867 (1967).
[5] J. O. M. Bockris, M. A. Genshaw, and M. Fullenwinder, Electrochim. Acta **15**, 47 (1970).
[6] L. Katz, M. Guinan, and R. J. Borg, Phys. Rev. B **4**, 330 (1971).
[7] J. Völkl and G. Alefeld, in *Hydrogen in Metals*, edited by G. Alefeld and J. Völkl (Springer, New York, 1978), p. 321.
[8] Y. Fukai, *The Metal-Hydrogen System* (Springer, Berlin, 2004).
[9] F. Buda, G. L. Chiarotti, R. Car, and M. Parrinello, Phys. Rev. Lett. **63**, 294 (1989).
[10] P. E. Blöchl, C. G. Van de Walle, and S. T. Pantelides, Phys. Rev. Lett. **64**, 1401 (1990).
[11] V. Milman, M. C. Payne, V. Heine, R. J. Needs, J. S. Lin, and M.

H. Lee, Phys. Rev. Lett. **70**, 2928 (1993).
[12] G. Lu, D. Orlikowski, I. Park, O. Politano, and E. Kaxiras, Phys. Rev. B **65**, 064102 (2002).
[13] D. E. Jiang and E. A. Carter, Phys. Rev. B **67**, 214103 (2003).
[14] P. G. Sundell and G. Wahnström, Phys. Rev. B **70**, 224301 (2004).
[15] B. Bhatia and D. S. Sholl, Phys. Rev. B **72**, 224302 (2005).
[16] A. Van der Ven and G. Ceder, Phys. Rev. Lett. **94**, 045901 (2005).
[17] D. S. Sholl, J. Alloys Compd. **446-447**, 462 (2007).
[18] H. Eyring, J. Chem. Phys. **3**, 107 (1935).
[19] C. Wert and C. Zener, Phys. Rev. **76**, 1169 (1949).
[20] G. Vineyard, J. Phys. Chem. Solids **3**, 121 (1957).
[21] P. Hohenberg and W. Kohn, Phys. Rev. **136**, B864 (1964); W. Kohn and L. J. Sham, *ibid.* **140**, A1133 (1965).
[22] O. Gunnarsson, B. I. Lundqvist, and S. Lundqvist, Solid State Commun. **11**, 149 (1972); U. von Barth and L. Hedin, J. Phys. C **5**, 1629 (1972) with the interpolation from S. H. Vosko, L. Wilk, and M. Nusair, Can. J. Phys. **58**, 1200 (1980).
[23] Y. Wang and J. P. Perdew, Phys. Rev. B **44**, 13298 (1991); J. P. Perdew, J. A. Chevary, S. H. Vosko, K. A. Jackson, M. R. Pederson, D. J. Singh, and C. Fiolhais, *ibid.* **46**, 6671 (1992).
[24] P. E. Blöchl, Phys. Rev. B **50**, 17953 (1994).
[25] G. Kresse and J. Hafner, Phys. Rev. B **47**, 558 (1993); G. Kresse and J. Furthmüller, *ibid.* **54**, 11169 (1996); G. Kresse and D. Joubert, *ibid.* **59**, 1758 (1999).
[26] K. Parlinski, Z. Q. Li, and Y. Kawazoe, Phys. Rev. Lett. **78**, 4063 (1997).
[27] MEDEA 2.3, Materials Design, Inc., Angel Fire, NM, USA, 2007.
[28] P. Pulay, Chem. Phys. Lett. **73**, 393 (1980).
[29] P. Piekarz, P. T. Jochym, K. Parlinski, and J. J. Łażewski, J. Chem. Phys. **117**, 3340 (2002).
[30] E. Tatge and H. E. Swanson, Natl. Bur. Stand. (U.S.) Circ. No. 539 359 (U.S. GPO, Washington, D.C., 1953), pp. I1–I95, as reported in the Inorganic Crystal Structure Data (ICSD) data base No. 64989.
[31] *CRC Materials Science and Engineering Handbook*, edited by J. Shackelford and W. Alexander (CRC, Ann Arbor, MI, 1992).
[32] T. G. Kollie, Phys. Rev. B **16**, 4872 (1977).
[33] M. L. Wayman and G. C. Weatherly, in *Binary Alloy Phase Diagrams*, 2nd ed., edited by T. B. Massalski (ASM International, Materials Park, OH, 1990), Vol. 2, p. 2047.
[34] C. H. Bennett, in *Diffusion in Solids: Recent Developments*, edited by A. S. Nowick and J. J. Burton (Academic, New York, 1975).
[35] A. F. Voter, Phys. Rev. Lett. **63**, 167 (1989).
[36] C. P. Flynn and A. M. Stoneham, Phys. Rev. B **1**, 3966 (1970).